Wave propagation in helically orthotropic elastic cylindrical shells and lattices

Sorokin, S.; Manconi, E.; Ledet, L.; Garziera, R.

Published in:
International Journal of Solids and Structures

DOI (link to publication from Publisher):
10.1016/j.ijsolstr.2019.04.031

Publication date:
2019

Document Version
Accepted author manuscript, peer reviewed version

WAVE PROPAGATION IN HELICALLY ORTHOTROPIC ELASTIC CYLINDRICAL SHELLS AND LATTICES

S. Sorokin , E. Manconi , L. Ledet , R. Garziera

PII: S0020-7683(19)30214-8
DOI: https://doi.org/10.1016/j.ijsolstr.2019.04.031
Reference: SAS 10359

To appear in: *International Journal of Solids and Structures*

Received date: 9 January 2019
Revised date: 4 April 2019

Please cite this article as: S. Sorokin , E. Manconi , L. Ledet , R. Garziera , WAVE PROPAGATION IN HELICALLY ORTHOTROPIC ELASTIC CYLINDRICAL SHELLS AND LATTICES, *International Journal of Solids and Structures* (2019), doi: https://doi.org/10.1016/j.ijsolstr.2019.04.031

WAVE PROPAGATION IN HELICALLY ORTHOTROPIC ELASTIC CYLINDRICAL SHELLS AND LATTICES

S. Sorokin[b], E. Manconi[a], L. Ledet[b], and R. Garziera[a]

[a] Dipartimento di Ingegneria e Architettura
Università degli Studi di Parma
Viale delle Scienze 181/A, 43100 Parma, Italy
e-mail: elisabetta.manconi@unipr.it

[b] Department of Materials and Production
Aalborg University
Fibigerstraede 16, DK-9220, Aalborg East, Denmark
e-mail: svs@m-tech.aau.dk

ABSTRACT

A use of orthotropic materials such as fibre-reinforced composites can introduce into vibro-acoustic performance of structures of canonical shape effects, not feasible when an isotropic material is used. In this paper, free and forced wave propagation in cylindrical structures with helically orthotropic material properties is analysed to demonstrate these effects. Two models, a thin cylindrical shell and a cylindrical beam lattice, are considered and two methods, an analytical method of the thin shell theory and a numerical Wave Finite Element method, are used. For both models, the symmetry break effect concerned with the location of dispersion curves is captured by means of these methods and explained. The influence of the helix angle and of the material parameters on the location of dispersion curves is investigated. The Green's matrix is formulated for rotating forces and the forcing problems are solved to highlight some unusual waveguide properties of the helically orthotropic cylindrical structures. The results are discussed in view of a possible application for control of energy flow in piping systems exposed to rotating excitation.

Keywords: helical structures, wave propagation, dispersion curves, Green's matrix, rotating forces, energy flow

1. INTRODUCTION

Wave propagation in helical waveguides has been a subject of interest since a long time ago, e.g. [1], and, as for many other research subjects, many original and interesting studies and applications can be found in the literature. Due to difficulties in solving partial differential equations for helical structures, in recent years there has been an increased interest in numerical methods for the analysis of wave propagation in helical waveguides, in particular, due to developments in structural health monitoring techniques. Dispersion curves in helical springs were obtained in [2] applying an asymptotic analysis and then the dominant balance method. Natural frequencies in helical spring were calculated in [3] using a dynamic stiffness method, while vibrations were studied in [4] applying a pseudo-spectral method and in [5] using the Green's matrix the Boundary Integral Method. Several numerical methods based on Finite Element discretization have been also proposed, each one showing some advantages or disadvantages with respect to the other. Vibration of helical springs with non-uniform ends was studied in [6] using a hybrid Wave Finite Element method. In [7] a Semi Analytical Finite Element method, based on translational invariance of curved waveguides, was presented, while in [8] dispersion curves were obtained based on the Scaled Boundary Finite Element. A Spectral Finite Element method was also recently applied for investigation of wave propagation in piezoelectric helical waveguide [9].

Wave propagation in elastic cylindrical shells has been studied in numerous publications. The vast majority of those are concerned with shells made of an isotropic material. Orthotropic shells have been considered in much fewer publications and the principal directions of tensor of elastic constants are customarily taken as coinciding with the cylindrical system of coordinates. It has been shown that all qualitative features of dispersion curves known for isotropic shells are preserved with some quantitative changes in magnitudes of cut-on frequencies, which, obviously, become dependent upon the ratio of elastic moduli in principal directions. A detailed survey of the literature on wave propagation in an orthotropic elastic shell lies beyond the scope of this paper, but the state-of-the-art in this area can be found in [10]. Recent advances in this area are highlighted in [11].

The technology of manufacturing of elastic pipes (cylindrical shells) for some technical applications, however, is such that the principal directions of the tensor of elastic constants are turned at a certain angle α to the cylindrical system of coordinates. This angle is kept constant along the length of a pipe so that fibres in a ply are helically wounded at the cylindrical surface. Often, an orthotropic cylindrical shell is made of many plies and the pitch angle for consecutive plies is switched to the opposite. By these means, the principal directions of elastic properties become aliened to the

cylindrical coordinate system. In the cases, when an odd number of plies is used and this number is small, the pitch angle affects the waveguide properties of the shell. Rather surprisingly, just a few publications dealing with helical waves and helically orthotropic cylindrical shells have been found by the authors. Specifically, helical waves in an isotropic elastic cylindrical shell have been considered in [12]. In this reference, the circumferential wave number has been treated as not necessarily integral, and, depending upon a chosen direction of propagation of the helical wave, dispersion equation has different solutions. References [13-14] are concerned with the wave propagation in a helically orthotropic cylindrical shell. However, most of the results of wave propagation analysis presented in these referenced are obtained for the axisymmetric wave. Bending vibrations are considered only for 'semi-infinite' shells. Therefore, we conclude that, to the best of our knowledge, propagation of non-axisymmetric waves in elastic cylindrical shells with helical orthotropy has not yet been properly analysed and this task constitutes the research goal and the novelty of this paper. Furthermore, in various technical applications thin elastic cylindrical shells (pipes) are exposed to time-harmonic rotating forces. We are unaware of any publications dealing with the analysis of energy flow generated by such forces in a helically orthotropic shell, and consider such an analysis as yet another aspect of novelty of our work.

The paper is structured as follows. Section 2 is concerned with the analytical model of wave propagation in a thin helically orthotropic cylindrical shell. In Section 3, this model is validated firstly by comparison of the dispersion diagrams with those presented in [11] for 'conventional' orthotropic shell. Second, the Wave Finite Element model is used for numerical analysis of wave propagation in a structure with helical geometry [15] and an agreement between numerical and analytical results is demonstrated. Section 3 also presents parametric studies of free waves in helically orthotropic cylindrical shells. In Section 4, a lattice beam model featuring the helical pattern is analysed to confirm the results obtained in the previous Section. The Green's matrix for a cylindrical shell with helical orthotropy is derived and used for analysis of the energy flow generated by a rotating force in Section 5. Novel findings of the paper are summarized in Section 6.

2. THE ANALYTICAL MODEL OF PROPAGATION OF SPINNING WAVES IN A THIN HELICALLY ORTHOTROPIC ELASTIC CYLINDRICAL SHELL

The governing equations of time-harmonic dynamics of a thin elastic cylindrical shell in the cylindrical coordinates (x, r, θ), with time-dependence taken as $\exp(-i\omega t)$ and this multiplier being omitted, are written following Gol'denweizer-Novozhilov theory [16,17]:

$$\frac{\partial N_x(x,\theta)}{\partial x}+\frac{1}{R}\frac{\partial S_{x\theta}(x,\theta)}{\partial \theta}+\rho h\omega^2 u(x,\theta)=q_x$$

$$\frac{1}{R}\frac{\partial N_\theta(x,\theta)}{\partial \theta}+\frac{\partial S_{x\theta}(x,\theta)}{\partial x}+\frac{1}{R}\frac{\partial M_\theta(x,\theta)}{\partial \theta}+2\frac{\partial H_{x\theta}(x,\theta)}{\partial x}+\rho h\omega^2 v(x,\theta)=q_x \qquad (1)$$

$$-\frac{1}{R}N_\theta(x,\theta)+\frac{\partial^2 M_x(x,\theta)}{\partial x^2}+2\frac{1}{R}\frac{\partial^2 H_{x\theta}(x,\theta)}{\partial x\partial \theta}+\frac{1}{R^2}\frac{\partial^2 M_\theta(x,\theta)}{\partial \theta^2}+\rho h\omega^2 w(x,\theta)=q_n$$

The components of deformation in the cylindrical coordinates are

$$\varepsilon_x=\frac{\partial u(x,\theta)}{\partial x},\ \varepsilon_\theta=\frac{1}{R}\frac{\partial v(x,\theta)}{\partial \theta}+\frac{w(x,\theta)}{R},\ \varepsilon_{x\theta}=\frac{1}{2}\left(\frac{1}{R}\frac{\partial u(x,\theta)}{\partial \theta}+\frac{\partial v(x,\theta)}{\partial x}\right) \qquad (2)$$

$$\kappa_x=-\frac{\partial^2 w(x,\theta)}{\partial x^2},\ \kappa_{\theta x}=-\frac{1}{R^2}\frac{\partial^2 w(x,\theta)}{\partial \theta^2}+\frac{1}{R}\frac{\partial v(x,\theta)}{\partial \theta},\ \kappa_{\theta x}=-\frac{1}{R}\frac{\partial w(x,\theta)}{\partial \theta \partial x}+\frac{\partial v(x,\theta)}{\partial x}$$

The principal directions of orthotropy of shell's material are turned by the angle α to the in-plane coordinates (x,θ) and constitute another orthogonal system (y,ψ), so that x coincides with y and θ coincides with ψ when $\alpha=0$. It is convenient to write the Hooke's law in the system (y,ψ), see Eqs. 14.13, p.55 in [18] (note the inverted indices in notations for Poisson ratio):

$$N_y=\frac{E_1 h}{1-\nu_{21}\nu_{12}}\left(\varepsilon_y+\nu_{12}\frac{E_2}{E_1}\varepsilon_\psi\right),\ N_\psi=\frac{E_2 h}{1-\nu_{21}\nu_{12}}\left(\nu_{12}\varepsilon_y+\varepsilon_\psi\right),\ S_{y\psi}=2G_e\varepsilon_{y\psi}$$

$$M_y=\frac{E_1 h^3}{12\left(1-\nu_{21}\nu_{12}\right)}\left(\kappa_y+\nu_{12}\frac{E_2}{E_1}\kappa_\psi\right),\ M_\psi=\frac{E_2 h^3}{12\left(1-\nu_{21}\nu_{12}\right)}\left(\nu_{12}\kappa_y+\kappa_\psi\right),\ H_{y\psi}=\frac{G_e h^3}{6}\kappa_{y\psi} \qquad (3)$$

The relations between components of deformation in these systems of coordinates are (see Eqs. 2.72-2.73, p.74 in [19]):

$$\varepsilon_y=\varepsilon_x\cos^2\alpha+\varepsilon_\theta\sin^2\alpha+2\varepsilon_{x\theta}\cos\alpha\sin\alpha$$

$$\varepsilon_\psi=\varepsilon_x\sin^2\alpha+\varepsilon_\theta\cos^2\alpha-2\varepsilon_{x\theta}\cos\alpha\sin\alpha$$

$$\varepsilon_{y\psi}=-\varepsilon_x\cos\alpha\sin\alpha+\varepsilon_\theta\cos\alpha\sin\alpha+2\varepsilon_{x\theta}\left(\cos^2\alpha-\sin^2\alpha\right) \qquad (4)$$

$$\kappa_y=\kappa_x\cos^2\alpha+\kappa_\theta\sin^2\alpha+2\kappa_{x\theta}\cos\alpha\sin\alpha$$

$$\kappa_\psi=\kappa_x\sin^2\alpha+\kappa_\theta\cos^2\alpha-2\kappa_{x\theta}\cos\alpha\sin\alpha$$

$$\kappa_{y\psi} = -\kappa_x \cos\alpha \sin\alpha + \kappa_\theta \cos\alpha \sin\alpha + 2\kappa_{x\theta}\left(\cos^2\alpha - \sin^2\alpha\right)$$

Respectively, the forces and moments in the (y,ψ) system are related to their counterparts in the (x,θ) coordinates as follows:

$$\begin{aligned}
N_y &= N_x \cos^2\alpha + N_\theta \sin^2\alpha + 2S_{x\theta}\cos\alpha\sin\alpha \\
N_\psi &= N_x \sin^2\alpha + N_\theta \cos^2\alpha - 2S_{x\theta}\cos\alpha\sin\alpha \\
S_{y\psi} &= -N_x \cos\alpha \sin\alpha + N_\theta \cos\alpha \sin\alpha + 2S_{x\theta}\left(\cos^2\alpha - \sin^2\alpha\right) \\
M_y &= M_x \cos^2\alpha + M_\theta \sin^2\alpha + 2H_{x\theta}\cos\alpha\sin\alpha \\
M_\psi &= M_x \sin^2\alpha + M_\theta \cos^2\alpha - 2H_{x\theta}\cos\alpha\sin\alpha \\
H_{y\psi} &= -M_x \cos\alpha \sin\alpha + M_\theta \cos\alpha \sin\alpha + 2H_{x\theta}\left(\cos^2\alpha - \sin^2\alpha\right)
\end{aligned} \tag{5}$$

Eqs. (2, 4-5) are substituted to the constitutive Eq. (3) and solved for $N_x, N_\theta, S_{x\theta}$ and $M_x, M_\theta, H_{x\theta}$. By these means, the forces and moments in cylindrical coordinates (x,θ) are expressed via displacements and their derivatives in the same system, while the Hooke's law has been formulated in helical coordinates (y,ψ), see Eqs. 16.2, p.62 in [18] or Eqs. 2.84-2.85, p.77 in [19]. Eventually, the forces and moments are substituted to Eq. (1) to yield the governing equations of wave motion in an infinite cylindrical shell with helical orthotropy in coordinates (x,θ). These equations are very cumbersome, and, therefore, not presented here. The derivation has been done in the analytical form by means of the symbolic manipulator Mathematica. It has been checked by the same means that setting $\alpha = 0$ gives conventional equations for an orthotropic cylindrical shell with the principal directions coinciding with the coordinate axes. Setting elastic moduli to their values for an isotropic material gives equations for an isotropic shell for any value of α.

This system of differential equations allows solution in the form

$$\begin{aligned}
u(x,\theta) &= U \exp\left(ikx + im\theta\right) \\
v(x,\theta) &= V \exp\left(ikx + im\theta\right) \\
w(x,\theta) &= W \exp\left(ikx + im\theta\right)
\end{aligned} \tag{6}$$

Substitution of Eqs. (6) in the governing equations and equating to zero the determinant of the system of linear algebraic equations with respect to the amplitudes (U,V,W) yields the dispersion equation in the polynomial form. The polynomial is of the sixth order in the frequency parameter and of the eighth order in wavenumber. As soon as $\alpha \neq 0$ it contains both the even and the odd powers of a wavenumber, that suggests the difference between the characteristics of waves travelling along the shell in opposite directions.

In Eq. (6), the integral circumferential wavenumber m may be both positive and negative. With the time-dependence in the form $\exp(-i\omega t)$, positive wavenumbers k found from the dispersion equation for a positive m describe waves travelling in the positive direction of the shell's axis and rotating clockwise. If a negative circumferential wavenumber is plugged in the dispersion equation, then positive wavenumbers describe waves travelling in the positive direction of the shell's axis and rotating anti-clockwise. It should also be noted that the conventional solution, which describes waves travelling without rotation along the axis of an orthotropic shell, i.e.,

$$\begin{aligned} u(x,\theta) &= U\exp(ikx)\cos(m\theta) \\ v(x,\theta) &= V\exp(ikx)\sin(m\theta) \\ w(x,\theta) &= W\exp(ikx)\cos(m\theta) \end{aligned} \qquad (7)$$

does not allow separation of trigonometric functions in the governing equations. This separation is recovered, when either the elastic parameters describe the isotropic shell, or $\alpha = 0$. Therefore, we conclude that standing in the circumferential direction waves cannot propagate in an orthotropic cylindrical shell with $\alpha \neq 0$. On the other hand, solution in the form (6) for an isotropic cylindrical shell allows separation of exponents in circumferential coordinate in the governing equations at any α. The resulting dispersion equation remains the same as when the conventional form of solution (7) is used. It means that the properties of spinning and standing in the circumferential coordinate waves are the same for an isotropic cylindrical shell. It is well-known and reported in classical texts on the dynamics of these shells.

3. DISPERSION DIAGRAMS: VALIDATION AND DISCUSSION

In this section, the model introduced in previous sections is verified, and waveguide characteristics of cylindrical shells with helically orthotropic material properties are discussed. In the following,

dispersion diagrams are plotted in the non-dimensional form with $k = k_{\text{dim}} R$ and $\Omega = \omega R \sqrt{\frac{\rho(1-\nu_{12}\nu_{21})}{E_1}}$.

3.1 Verification of the analytical model of an orthotropic cylindrical shell

We begin with a validation of the model of an orthotropic shell for the case, when principal directions of orthotropy coincide with the cylindrical coordinates, i.e., when $\alpha = 0$. The parameters of a shell are taken as in [11], Eq.8, p.25: $E_x = E_1 = 207\,\text{GPa}$, $E_\theta = E_2 = 5\,\text{GPa}$, $G_{x\theta} = G_{12} = 2.6\,\text{GPa}$, $\nu_{x\theta} = \nu_{12} = 0.25$, $\frac{h}{R} = 0.1$, $m = 2$.

The branches corresponding to propagating waves (purely real wavenumbers) and to the evanescent waves (purely imaginary wavenumbers) are marked dark blue and red (in this order). The real parts of complex wavenumbers of attenuated waves are marked light blue, and their imaginary parts are marked magenta. In [11], Fig. 1, page 26, only purely real wavenumbers are presented. Fig. 1 in this paper provides a more detailed dispersion diagram, in which purely imaginary and complex-valued wavenumbers are also shown. There is a perfect agreement between characteristics of propagating waves in these two Figures. In particular, the cut-on frequencies are exactly the same: $\Omega_{cut-on,1} = 0.012026$, $\Omega_{cut-on,2} = 0.22415$, $\Omega_{cut-on,3} = 0.34789$. In the case $\alpha = 0$, the dispersion equation contains only even powers of wavenumber and features the symmetry of the dispersion diagram with respect to the frequency axis. Therefore, the common practice to show only its upper part, i.e., $\text{Re}[k] \geq 0$, $\text{Im}[k] \geq 0$ is followed in Fig. 1.

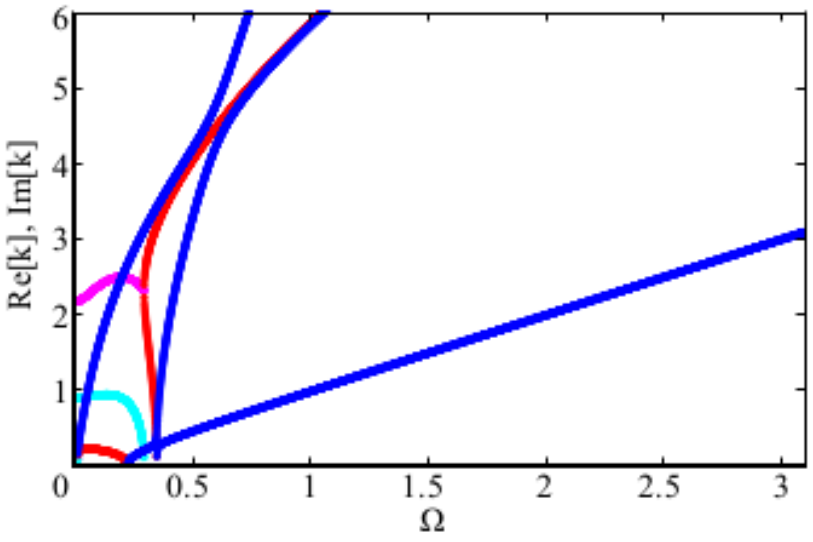

Fig. 1. Verification in comparison with Fig.1 from [11], Fig.1, p.26.

As soon as $\alpha \neq 0$, the symmetry is broken. This is illustrated in Fig. 2 for a shell with the same parameters as in the previous case, but with $\alpha = \frac{\pi}{6}$. The colours are used in the same way as in Fig. 1. It is more convenient to present the dispersion diagram in 3D as is done in Fig. 2(b).

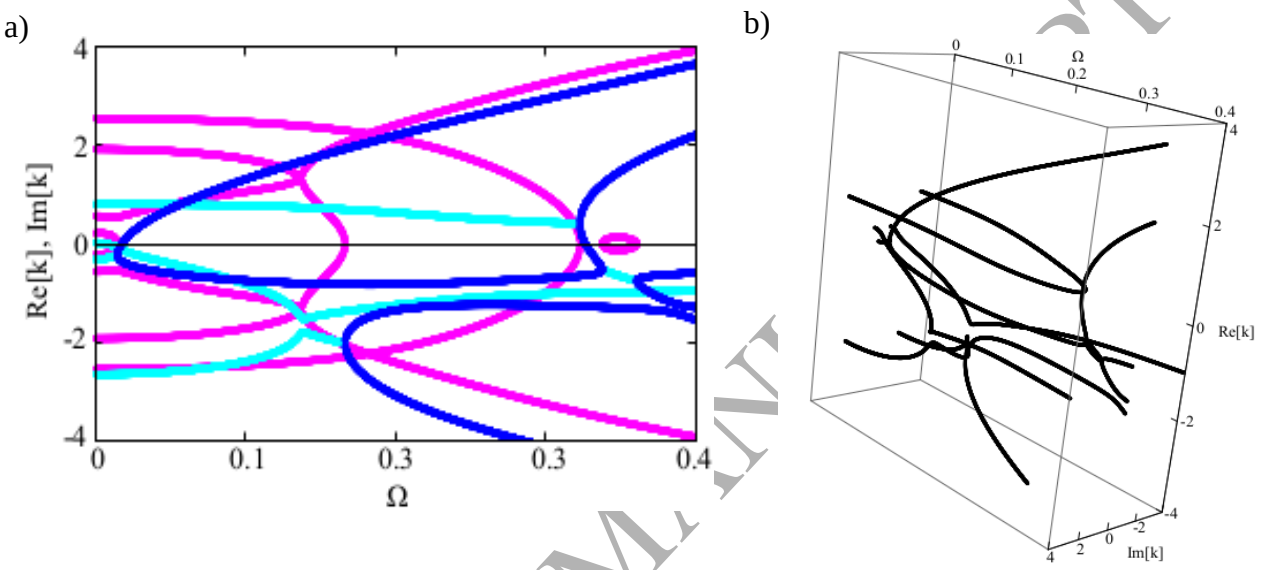

Fig. 2. (a) dispersion diagram for the shell with the same parameters as in [11] and $\alpha = \frac{\pi}{6}$*; (b) 3D presentation of the dispersion diagram.*

This diagram features the classical veering effect in the frequency range $0.135 < \Omega < 0.145$ and the classical locking effect in the frequency range $0.34 < \Omega < 0.36$ (see [20,21]), but, more importantly, the unevenness of frequency-dependence of wavenumbers, which describe waves moving with anti-clockwise rotation in the positive and negative directions of the axial coordinate. It manifests itself as the non-symmetry of the location of dispersion curves with respect to the plane $\mathrm{Re}[k] = 0$. On the other hand, it is straightforward to check that there is the symmetry with respect to this plane between the dispersion curves for ($m = 2$, $\alpha = \frac{\pi}{6}$) and the dispersion curves for ($m = 2$, $\alpha = -\frac{\pi}{6}$).

Likewise, the symmetry is preserved for the dispersion curves plotted for ($m=2, \alpha=\frac{\pi}{6}$) and ($m=-2, \alpha=\frac{\pi}{6}$). This is readily explained by the simple observation that the waves travelling in the positive direction of the *x*-axis and rotating anticlockwise are identical to the waves travelling in the negative direction of the *x*-axis and rotating clockwise (if this rotation is viewed from the same point) or vice-versa.

3.2 Comparison of results obtained by means of the analytical model and the wave finite element method

The results, presented in the previous sub-section, have conclusively validated the analytical model of an orthotropic cylindrical shell in the case when the principal directions of orthotropy coincide with the axes of coordinates. Since no references, which present dispersion diagrams for an orthotropic shell with $\alpha \neq 0$, have been found we choose to validate this model for a helically orthotropic shell by calculations of wavenumbers by means of the Wave Finite Element method as presented in [15].

A pipe with thickness $h=0.01\,\text{m}$ and mean radius $R=0.2\,\text{m}$ (that gives $h/R=0.05$) is considered. Material properties are: $E_x=E_1=28.89\,\text{GPa}$, $E_\theta=E_2=9.63\,\text{GPa}$, $G_{x\theta}=G_{12}=4.128\,\text{GPa}$, $\nu_{x\theta}=\nu_{12}=0.06$ (this implies that $\nu_{\theta x}=\nu_{21}=0.02$), $\rho=1389\,\text{kg/m}^3$. The angle is $\alpha=\frac{\pi}{6}$. To apply the WFE approach the FE model of a small periodic segment of the pipe of length $L_x=L_x=0.002\,\text{m}$ is discretised using 5 solid elements; this model allows to obtain accurate results up to high frequency [15].

We note that the analytical model in Section 2 is based on the classical thin shell theory, whereas the finite element model is constructed by means of 3D solid elements in the framework of the commercially available software ANSYS. Therefore, the agreement between results obtained by use of these so profoundly different models should be regarded as the strong indication of the correctness of the both. However, some discrepancies are likely to occur due to the difference between modelling methods. The results are presented in Table 1 for two circumferential wavenumbers and two excitation frequencies. As seen from this Table, the differences are small and should be attributed to the difference in formulations of constitutive relations in the finite element and analytical models. The detailed convergence studies and comparison of validity ranges of the models do not constitute the goal of this paper. We just note that the closeness of the wavenumbers to each

other suggests that both models are applicable to the analysis of wave propagation in helically orthotropic cylindrical shells.

As already mentioned, the remarkable feature of these results is the unevenness of purely real wavenumbers (those corresponding to travelling waves) presented in the first two columns of the Table. In what follows in this Section, we briefly explore the influence of geometry and material parameters on the location of dispersion curves by means of the analytical model. It is a straightforward matter to show that the dispersion polynomial at the 'breathing mode' $m=0$ does not contain odd powers of the wavenumber for any α regardless the helical orthotropy. The difference of wave propagation in a helically orthotropic cylindrical shell from the same shell with $\alpha=0$ is the coupling purely torsional and longitudinal-flexural axisymmetric deformation. In that follows, we do not elaborate on this issue and do not consider this mode any further. On the other hand, the performance of a helically orthotropic shell at any other circumferential wavenumber is qualitatively the same. Therefore, we restrict our subsequent analysis to the case $m=1$.

3.3 The influence of the geometry parameter α

In Fig. 3(a), the non-dimensional parameters are chosen as $\frac{E_2}{E_1}=8$, $\nu_{12}=0.3$ $\frac{G_{12}}{E_1}=0.35$, $\frac{h}{R}=0.05$.

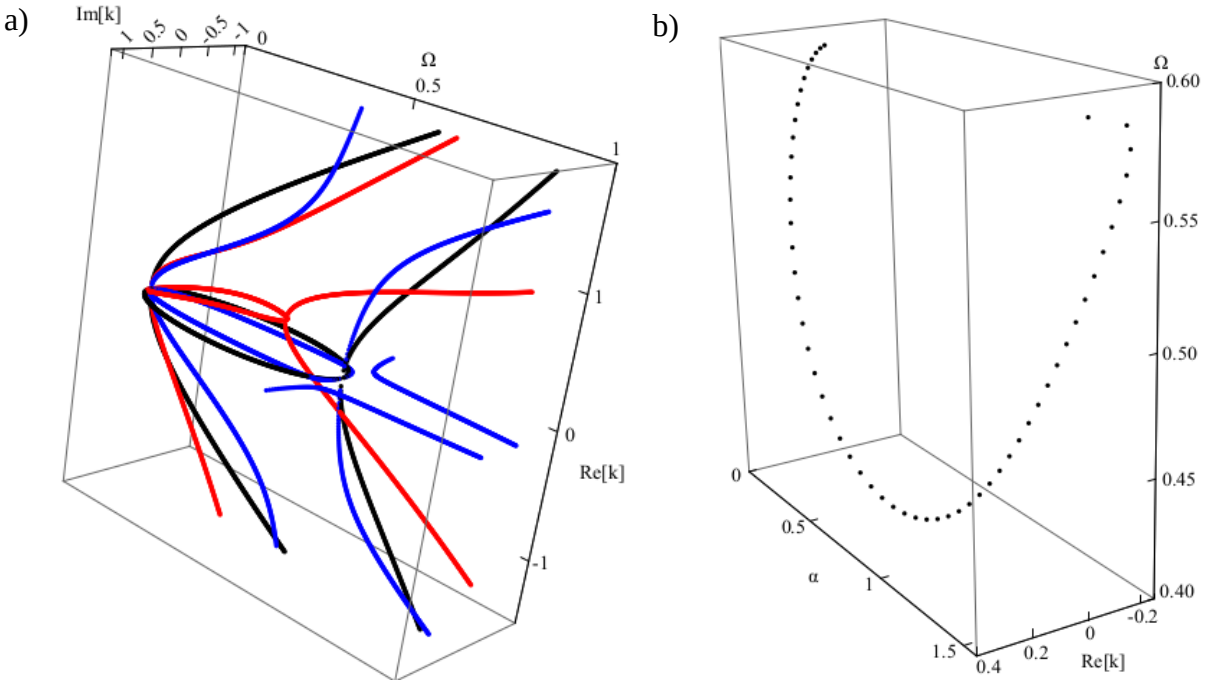

Black curves are plotted for $\alpha = 0$ blue ones for $\alpha = \frac{\pi}{2}$ and red ones for $\alpha = \frac{\pi}{4}$.

Fig. 3. (a) dispersion diagram for $\alpha = 0$ (black), $\alpha = \frac{\pi}{4}$ (red), $\alpha = \frac{\pi}{2}$ (blue); (b) the second cut-on frequency and associated purely real wavenumber, at which the group velocity is zero versus the orthotropy angle.

To begin with, it should be noted that the dispersion diagram is shown in the range of complex-valued wavenumbers, in which not all eight branches can be seen. In particular, when $\alpha = \frac{\pi}{2}$, the two curves chopped at $\mathrm{Im}[k] = \pm 1$ may be traced to the plane $\Omega = 0$ in a broader window $(\mathrm{Re}[k], \mathrm{Im}[k])$. Only four branches are located within this range of $(\mathrm{Re}[k], \mathrm{Im}[k])$ at $\alpha = 0$ and $\alpha = \frac{\pi}{4}$. Naturally, at $\alpha = 0$ and $\alpha = \frac{\pi}{2}$ the dispersion diagrams are perfectly symmetric with respect to $\mathrm{Re}[k] = 0$ plane, and the second propagating wave cuts on in the standard 'divergence-type' manner at $k = 0$, $\Omega_{cut-on,2} = n\sqrt{\frac{G_{12}}{E_1}} = 0.5916$. This value of cut-on frequency is obtained analytically, and it is the same for both $\alpha = 0$ and $\alpha = \frac{\pi}{2}$. For $\alpha = \frac{\pi}{4}$, the scenario of this cut-on is different, and it is of 'flutter-type', which is well-known in the theory of elastic waves in layers and thin shells. As seen from Fig. 3, the transformation of two attenuated waves to two propagating ones occurs at $\Omega \approx 0.4152$, $k \approx 0.2264$ and the lower branch in the frequency range $0.4152 \le \Omega \le 0.4693$ describes the anomalous (or negative energy) wave, which has the positive phase velocity $c_{phase} > 0$ and negative group velocity $c_{group} < 0$. Remarkably, in the analogous symmetric waveguides (say, the second branch of symmetric waves in the Rayleigh-Lamb problem, see [22], Figure 5.072, p. 151) such waves exist in pairs, whereas here, due to the symmetry break, this wave does not have a counterpart of similar properties. In Fig. 3, the other branch emerging from $\Omega \approx 0.4152$, $k \approx 0.2264$ has both $c_{phase} > 0$, $c_{group} > 0$. This result is interesting on its own, but it also has some implications regarding solving the forcing problems in general and constructing the Green's matrix in particular. An elaboration on this important issue is presented in Section 5. The evolution of the cut-on

frequency for $0 < \alpha < \frac{\pi}{2}$ is illustrated in Fig. 3(b). Effectively, this figure presents a dependence of the position of a point (Ω_0, k_0) in the $(\Omega, \mathrm{Re}[k])$-plane, at which $c_{group} = 0$, upon the angle α. As

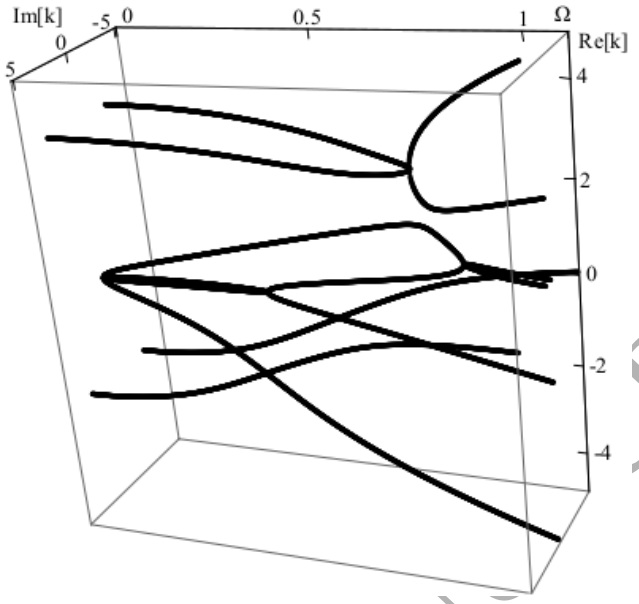

seen (also from Fig. 3), $\Omega_0 = \Omega_{cut-on,2}$, $k_0 = 0$ at both extreme values $\alpha = 0$ and $\alpha = \frac{\pi}{2}$. The dependence of (Ω_0, k_0) upon the angle α is not monotonic and, for the given parameters of orthotropy, the angle $\alpha = \frac{\pi}{4}$ does not appear to be the one, at which the dispersion diagram is maximally distorted. Fig. 3(b) shows that the second wave at $\alpha \approx 1.0755$ cuts-on when $k_0 = 0$. However, this does not mean that the whole dispersion diagram recovers symmetry, see Fig. 4.

Fig. 4. Dispersion diagram for $\alpha \approx 1.0755$.

In this figure, all branches of the dispersion diagram are plotted. Despite conventional 'divergence' type generation of the second propagating waves, the diagram is lacking symmetry with respect to $\mathrm{Re}[k] = 0$ plane. In the considered frequency range, there are two waves propagating in the negative direction of the axial coordinate that do not experience any transformations. The situation is different with waves travelling in the positive direction: at around $\Omega = 0.78$ two propagating waves cut on. One of these waves interacts with the first propagating wave in the 'veering' manner (see [20]) and, due to 'repelling', interacts with the second branch in the 'locking' manner. Therefore, in the frequency range $0.815 \le \Omega \le 0.931$ this waveguide supports four waves with positive phase velocities. Two of these waves have negative group velocities. This result has a potential for tailoring

the waveguide properties of helically orthotropic cylindrical shells and, as already mentioned, is considered in Section 5, where the problem of excitation of elastic waves in a shell by a rotating force is solved.

3.4 The influence of the parameters of orthotropy

Obviously, the parameters of orthotropy strongly affect the location of dispersion curves, and variation of the angle α adds one more dimension to the space of parameters. Therefore, the analysis reported in this subsection is purely illustrative and highlights the influence of the stiffness ratios $\frac{E_2}{E_1}$ and $\frac{G_{12}}{E_1}$ with other ones being fixed to the values used in subsection 3.2: $\nu_{12}=0.3$, $\frac{h}{R}=0.05$. In addition, $\alpha=\frac{\pi}{4}$. It is important to observe the limitations on the values of the parameter $\frac{E_2}{E_1}$, see Eq. 7, p. 25, [10]. For $\nu_{12}=0.3$, the limitation is $\frac{E_2}{E_1}<11$. In Fig. 5(a), the influence of this parameter is illustrated for $\frac{G_{12}}{E_1}=0.35$. As expected, the reverse change in the ratio $\frac{E_2}{E_1}$ tends the

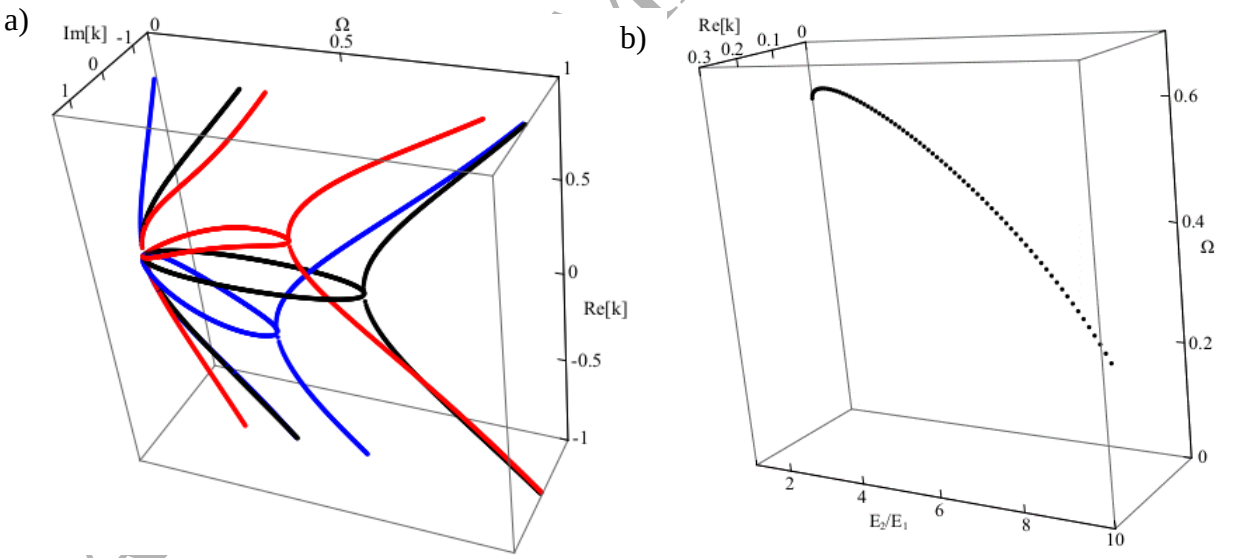

diagram in the opposite directions. The quantitative differences between cases $\frac{E_2}{E_1}=8$ and $\frac{E_2}{E_1}=\frac{1}{8}$ are explained by, firstly, the scaling of the frequency parameter with E_1 in both cases and, secondly, by fixation $\nu_{12}=0.3$.

Fig. 5. (a) dispersion diagrams for $\frac{E_2}{E_1}=1$ (black), $\frac{E_2}{E_1}=8$ (red), $\frac{E_2}{E_1}=\frac{1}{8}$ (blue); (b) the second cut-on frequency and associated purely real wavenumber versus $\frac{E_2}{E_1}$.

Fully reversed choice of parameters gives the dispersion diagram 'mirrored' with respect to the plane $\mathrm{Re}[k]=0$. The dispersion diagram is recovered completely if, in addition to the rescaling of the frequency parameter and fixing ν_{21}, the circumferential wavenumber is set to be $m=-1$. In Fig. 5(b), the dependence of the position of a point (Ω_0, k_0) in the $(\Omega, \mathrm{Re}[k])$-plane, at which $c_{group}=0$, upon the ratio $\frac{E_2}{E_1}$ is illustrated.

Finally, we illustrate the influence of the shear stiffness parameter $\frac{G_{12}}{E_1}$ in Fig. 6 with other ones being fixed to the values used in subsection 4.3: $\nu_{12}=0.3$ $\frac{E_2}{E_1}=8$ $\frac{h}{R}=0.05$, $\alpha=\frac{\pi}{4}$. This parameter also strongly influences the location of dispersion curves and triggers veering and locking interaction phenomena.

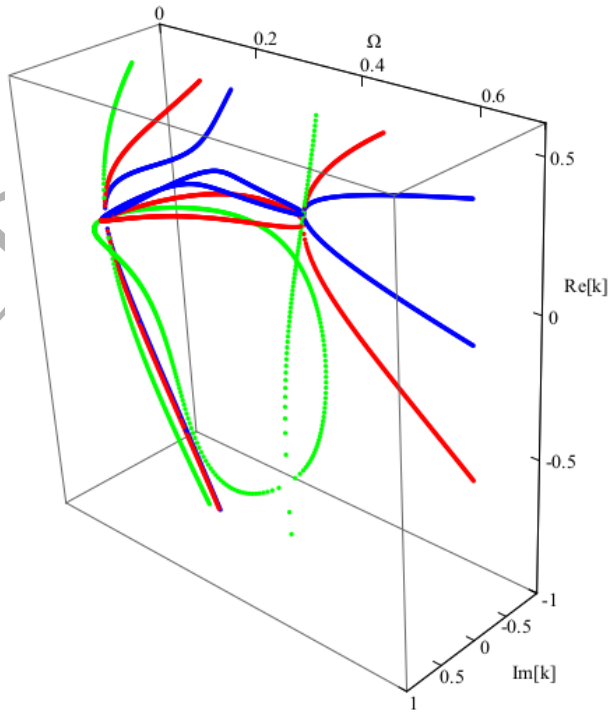

Fig. 6. Dispersion diagram for $\frac{G_{12}}{E_1} = 0.35$ (red), $\frac{G_{12}}{E_1} = 3.5$ (green) and $\frac{G_{12}}{E_1} = 0.035$ (blue)

To conclude this brief analysis of dispersion diagrams of cylindrical shell with the helical orthotropy, we notice that the symmetry of dispersion curves remains preserved with respect to the $\mathrm{Im}[k] = 0$ plane. In other words, the complex-valued and purely imaginary roots exist only in complex conjugate pairs simply because the dispersion polynomial has purely real coefficients in the absence of damping.

4. WAVES IN A CYLINDRICAL BEAM LATTICE WITH HELICAL PATTERN

As shown in the previous Section, wave propagation in a helically orthotropic cylindrical shell is associated with spinning and waveguide properties of a shell are different depending upon the direction of rotation. Mathematically, it manifests itself as the presence of both even and odd powers of wavenumber in dispersion equation. On the other hand, as is well-known, the dispersion equation for a helical spring contains only even powers of wavenumber and, therefore, there is the symmetry in waveguide properties of an isolated helical fibre. It is realistic to assume that a helically orthotropic cylindrical shell is made of a fibre-reinforced composite, which consists of a large number of identical helical fibres uniformly embedded into a relatively soft matrix. A simplified discrete model of a shell may then be set up as a lattice of beam elements forming helical fibres with

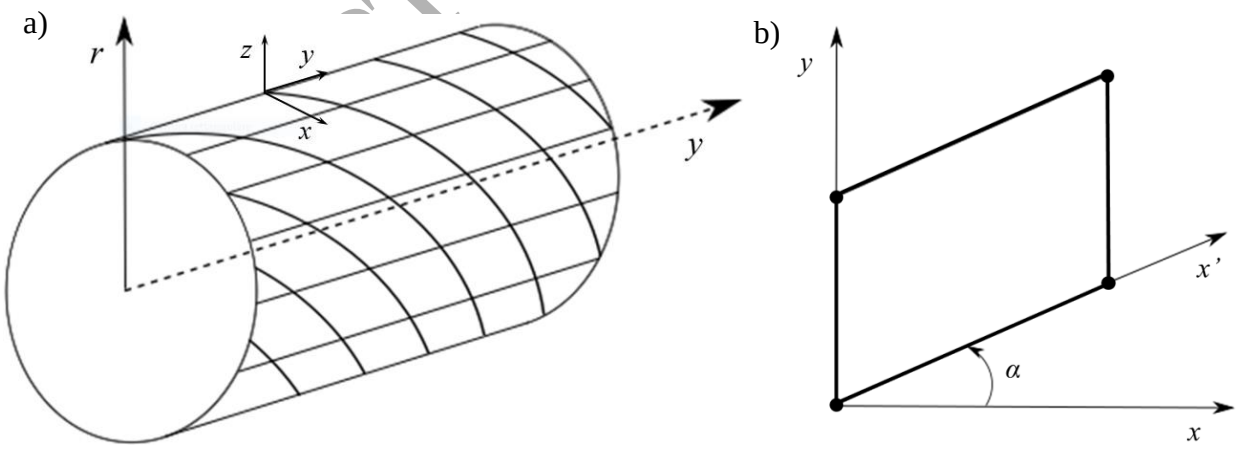

the matrix between them being modelled as discrete beams of lower stiffness.

Fig. 7. (a) schematic representation of the cylindrical beam lattice with helical pattern; (b) the periodic unit cell.

In this section complex dispersion curves of an orthotropic lattice structure with helical pattern are shown. Lattice structures have been extensively studied due to their application in many engineering fields [23], and the investigation and optimization of their properties is still the subject of many recent studies. Amongst other studies, as an example, in [24] a homogenization of two-dimensional lattice has been presented, directionality behaviour of lattices has been investigated in [25], while in [26] stress wave in two-dimensional periodic lattices has been studied.

Floquet and Bloch analysis of a unit cell are particularly useful to investigate the behaviour of beam lattice structures, and the WFE method [15] can be straightforwardly applied, being the method an FE application of wave propagation in periodic structures. Although the interest here is not in bandgaps formation of the lattice, e.g. [27], and bandgaps are not showed and discussed in this section, these can be also easily investigated using the present approach. Figure 7 shows a schematic representation of the helical lattice considered, together with the unit periodic cell assumed for the WFE discrestisation [15]. The latter is modelled using beam elements with six degrees of freedom per node: displacements and rotations in the *x*, *y* and *z* directions. Orthotropy is assumed such that Young's modulus in the *y* direction is three time those in the helical direction, that is: $E_y / E_{x'} = 3$.

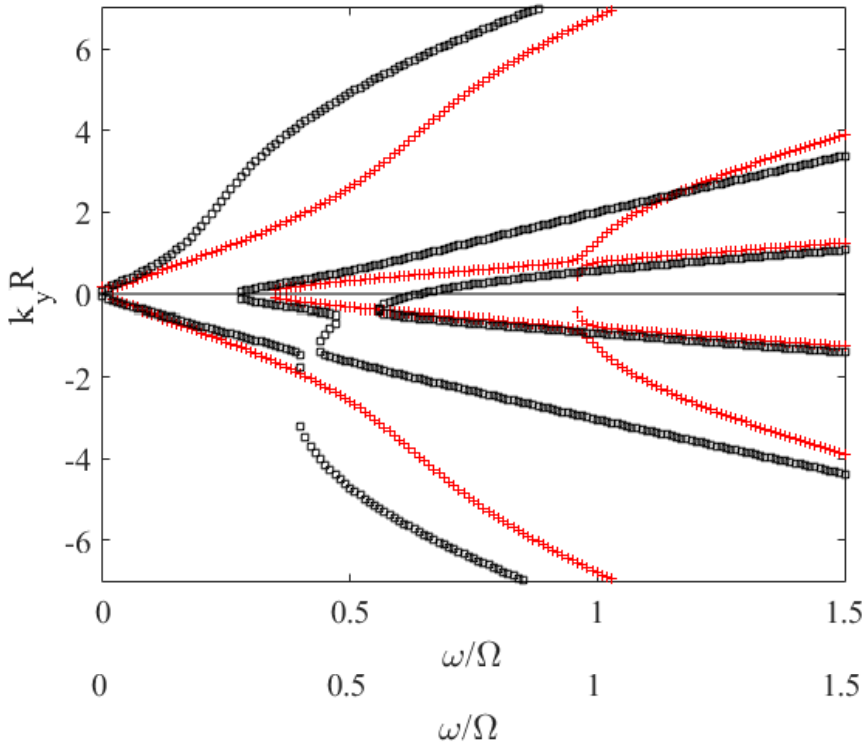

The radius o ircumference; the beam cross section is square 0.01x0.01m, and the helix angle is $\alpha = \pi / 4$.

Fig. 8. comparison between the real-valued dispersion curves for the cylindrical beam lattice, first circumferential mode m=1: +++ orthotropic cylindrical lattice (rectangular cell); □□□ orthotropic helical cylindrical lattice (skew cell).

The estimation of the differences between the orthotropic cylindrical lattice, viz. rectangular periodic cell, and the orthotropic cylindrical helical lattice, viz. skew periodic cell, is shown in Fig. 8, where the real valued dispersion curves for the first circumferential mode are compared. Dispersion curves

are plotted using the non-dimensional frequency and wavenumber according to Section 3. For the orthotropic cylindrical lattice, it can be seen that the curves show symmetry with respect to Re[k]=0 axis: wavenumbers occurs in pairs $\pm k$ and waves propagating in positive and negative axial direction have the same characteristics in terms of wavenumbers and wavemodes. It can also be noticed that quasi-extensional wave modes (the second branch in the plot) propagate below $\Omega = 1$. As the frequency increases the structure starts to be less stiff involving radial direction, the extensional wave mode changes in the behaviour due to transverse motion of the cross section, and a higher order mode asymmetric mode start propagating close to $\Omega = 1$ as expected.

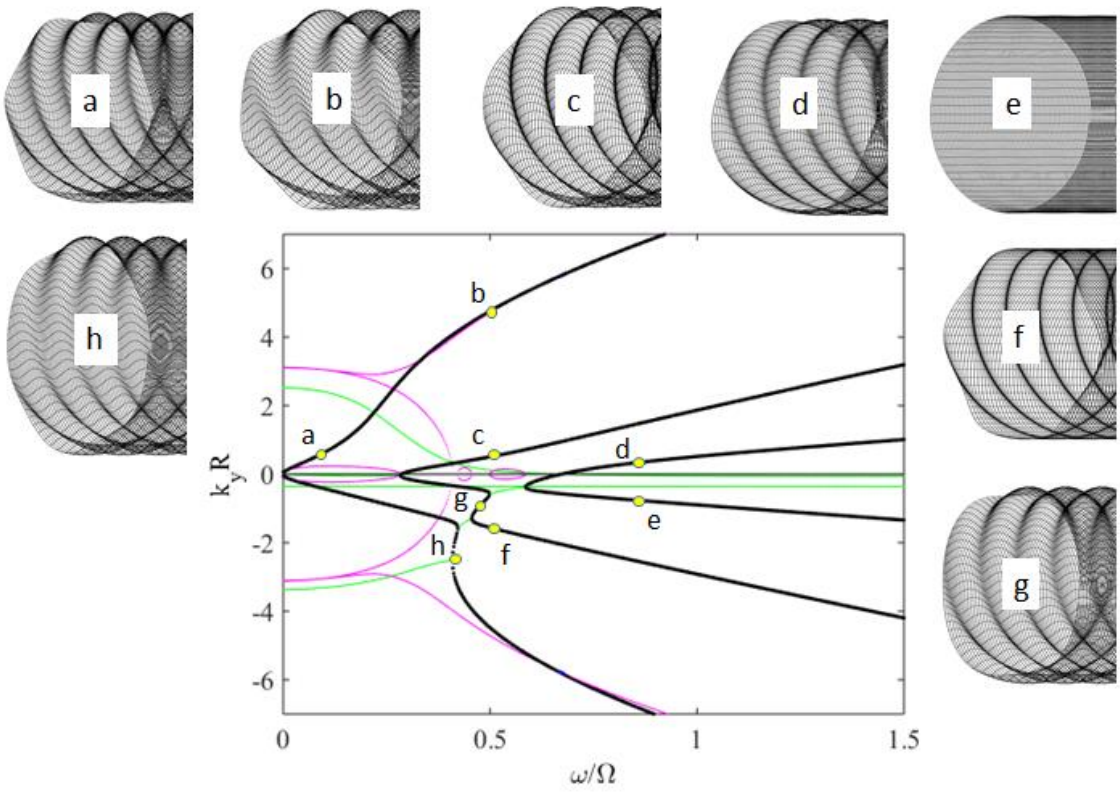

Fig. 9. Complex dispersion curves for the helical hortotropic cylindrical beam lattice, first circumferential mode m=1: —— propagating modes; —— evanescent modes; —— : complex modes (note that complex modes occur as a pair of complex conjugate modes, and only one of the pair is shown here). The inlet figures show the wave modes.

The figure shows clearly that the presence of the helical orthotropy highly affects the waves propagating in the lattice, which leads to changes in the cut-off frequencies and in the wave propagation properties as described in the previous sections: the symmetry in the location of dispersion curves no longer holds for and waves propagate differently in positive and negative

directions provided that the helical rotation is the same. Complex dispersion curves and some of the wavemodes for the orthotropic helical lattice are shown in Fig. 9. The latter shows the deformation of the lattice under the passage of the corresponding wave.

5. FORMULATION OF GREEN'S MATRIX AND ENERGY FLOW ANALYSIS

The analytical model formulated in Section 2 may readily be used for analysis of forced response of a cylindrical shell with helical orthotropy. The convenient tool to handle arbitrary excitation conditions is the Green's matrix. Since the studies of free spinning waves have demonstrated their unusual properties of non-symmetry, formulation of Green's matrix is particularly interesting for rotating forces, which are typical for various technical applications, such as water-supplying pipes with centrifugal pumps, wind turbines and other rotating machinery.

5.1 The loading cases

We consider time-harmonic, $\exp(-i\omega t)$, external forces of unit amplitude concentrated in the axial direction (i.e., applied at the cross-section $x = x_0$) and rotating in the circumferential direction:

$$q_m^{F(n)}(x - x_0, \theta) = \delta(x - x_0)\exp(im\theta), \; n = 1,2,3,4 \qquad (8)$$

Forcing at each circumferential wavenumber may be considered individually, and four loading cases $n = 1,2,3,4$ in Eq. (8) correspond to the action of an axial force, circumferential force, radial force and axial bending moment, respectively. Explicit formulas for these forces in the case of isotropic cylindrical are well-known and may be found, for instance, in [28], p. 821, Eqs. (6). However, in the case of helical orthotropy, the closed form analytical expressions become cumbersome so that we do not reproduce them here.

The derivation of Green's matrix is based on the modal decomposition on free waves. For an orthotropic cylindrical shell with the principal directions of orthotropy coinciding with cylindrical coordinates (i.e., for a symmetric waveguide), it is sufficient to formulate four loading conditions. These conditions, see [28], Section 4, ensure symmetry of the wave propagation pattern to the left and to the right of the loaded cross-section $x = x_0$. Respectively, four wavenumbers k_j ($j = 1,2,3,4$), each of which satisfies radiation/decay conditions, are used and the solution ansatz for the radial displacement in the loading case $q_m^{F(n)}(x - x_0, \theta)$ has the form $w_m^{F(n)}(x - x_0) = \sum_{j=1}^{4} A_{mj}^{(n)} \exp\left(ik_j |x - x_0|\right)$.

All other state variables (generalised forces and displacements) are expressed in the closed analytical

form via amplitudes $A_{mj}^{(n)}$ and wavenumbers k_j using the modal coefficients, for instance, $Q_{m1}^{F(n)}(x-x_0)=\sum_{j=1}^{4} M_{m1j} A_{mj}^{(n)} \exp\left(ik_j|x-x_0|\right)$, see details in [28].

As soon as the symmetry is broken (the helical orthotropy is considered), all eight wavenumbers should be involved in the formulation of Green's matrix and eight conditions at the loaded cross-section $x=x_0$ should be formulated. Specifically, each component of the displacement vector and three forces are continuous, while the remaining force experiences a unit jump. For the loading case 3 (rotating radial force) these conditions are:

$$w_{m+}^{F(3)}(0)=w_{m-}^{F(3)}(0), \quad u_{m+}^{F(3)}(0)=u_{m-}^{F(3)}(0), \quad v_{m+}^{F(3)}(0)=v_{m-}^{F(3)}(0), \quad \gamma_{m+}^{F(3)}(0)=\gamma_{m-}^{F(3)}(0)$$

$$Q_{m1+}^{F(3)}(0)=Q_{m1-}^{F(3)}(0), \quad Q_{m2+}^{F(3)}(0)=Q_{m2-}^{F(3)}(0), \quad Q_{m3+}^{F(3)}(0)=Q_{m3-}^{F(3)}(0)+1, \quad Q_{m4+}^{F(3)}(0)=Q_{m4-}^{F(3)}(0) \qquad (9)$$

Modal decomposition of the forced response in the region $x<x_0$ is done using free waves with wavenumbers which have $\mathrm{Im}(k_j^-)<0$, $j=1,2,3,4$ and, if $\mathrm{Im}(k_j^-)=0$, $\frac{d\omega}{dk_j^-}<0$:

$$w_{m-}^{F(n)}(x-x_0)=\sum_{j=1}^{4} A_{mj-}^{(n)} \exp\left(ik_j^-(x-x_0)\right).$$

In the region $x>x_0$, wavenumbers with $\mathrm{Im}(k_j^+)>0$ and, if $\mathrm{Im}(k_j^+)=0$, with $\frac{d\omega}{dk_j^+}>0$ are used:

$$w_{m+}^{F(n)}(x-x_0)=\sum_{j=1}^{4} A_{mj+}^{(n)} \exp\left(ik_j^+(x-x_0)\right).$$

As soon as $\alpha=0$ or $\alpha=\frac{\pi}{2}$, wavenumbers satisfy the condition $k_j^-=-k_j^+$. Then the symmetry is recovered and the Green's matrix for rotating forces acquires the form known for the isotropic cylindrical shell.

5.2 The energy flow

The scaled energy flow through a cross-section of the shell is formulated as (see [28-30]):

$$N_{m+}^{(j)}=\frac{1}{2}\mathrm{Re}\Big\{Q_{m1+}^{F(j)}(x)\cdot\left[i\Omega u_{m1+}^{F(j)}(x)\right]^*+Q_{m2+}^{F(j)}(x)\cdot\left[i\Omega v_{m1+}^{F(j)}(x)\right]^*$$
$$+Q_{m3+}^{F(j)}(x)\cdot\left[i\Omega w_{m1+}^{F(j)}(x)\right]^*+Q_{m4+}^{F(j)}(x)\cdot\left[i\Omega\gamma_{m1+}^{F(j)}(x)\right]^*\Big\}, \qquad x>x_0 \qquad (10a)$$

$$N_{m+}^{(j)} = \frac{1}{2}\mathrm{Re}\Big\{Q_{m1+}^{F(j)}(x)\cdot\left[i\Omega u_{m1+}^{F(j)}(x)\right]^{*} + Q_{m2+}^{F(j)}(x)\cdot\left[i\Omega v_{m1+}^{F(j)}(x)\right]^{*}$$
$$+ Q_{m3-}^{F(j)}(x)\cdot\left[i\Omega w_{m-}^{F(j)}(x)\right]^{*} + Q_{m4-}^{F(j)}(x)\cdot\left[i\Omega \gamma_{m-}^{F(j)}(x)\right]^{*}\Big\}, \qquad x < x_0 \qquad (10b)$$

In an orthotropic case, when $\alpha = 0$ or $\alpha = \frac{\pi}{2}$, any force defined as Eq. (8) generates, similarly to an isotropic shell, the same energy flow in the regions $x < x_0$ and $x > x_0$, $N_{m-}^{(j)} = N_{m+}^{(j)}$. As soon as $\alpha \neq 0$, the energy input is not split into equal shares between these regions. This effect, introduced by the helical orthotropy, may be utilized to control the transmission of vibro-acoustic energy generated by rotating forces in various piping systems.

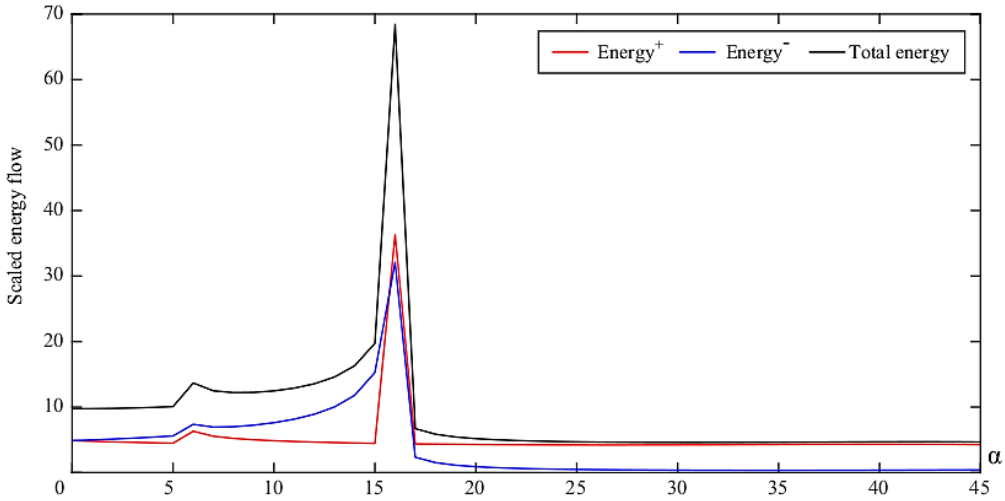

Fig. 10. The energy flow in a helically orthotropic cylindrical shell

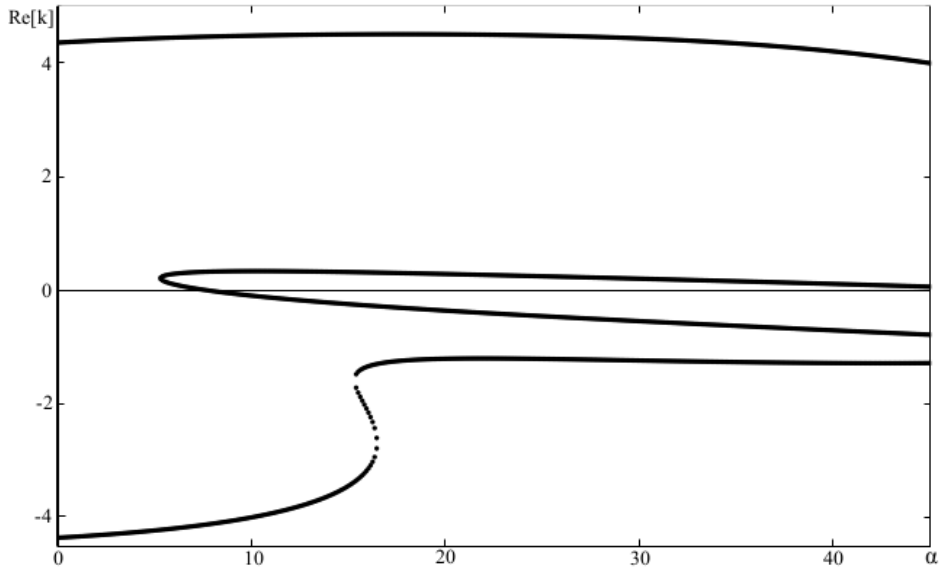

Fig. 11. The purely real wavenumbers at $\Omega = 0.4$ *as functions of the orthotropy angle* α.

We illustrate this effect for an orthotropic shell with parameters used in subsection 3.3: $\nu_{12} = 0.3$, $\frac{E_2}{E_1} = \frac{1}{8}$, $\frac{h}{R} = 0.05$, $\frac{G_{12}}{E_1} = 0.35$. We consider rotating radial force ($n = 3$) of unit amplitude with $m = 1$ at the excitation frequency $\Omega = 0.4$. The scaled energy flow as a function of the angle α is shown in Fig. 10, where α is measured in degrees and varies from $\alpha = 0$ to $\alpha = 45^0$ with the step of 1^0. To explain peaks in the energy input at the angles $\alpha \approx 5^0$ and $\alpha \approx 17^0$ it is necessary to address the dependence of purely real wavenumbers upon α at the frequency $\Omega = 0.4$, see Fig. 11.

When $\alpha \le 5^0$, there is only one pair of propagating waves, which have almost the same absolute values of purely real wavenumbers. Therefore, there is little difference in the energy flow in the positive and negative directions. This can be seen in Fig. 12(a), where the contributions to energy flow are presented versus the axial coordinate for $\alpha = 3^0$. It can also be noticed that a pair of propagating waves emerges (notably, not at the $k = 0$ axis, but rather following condition $\frac{d\omega}{dk} = 0$, attained when $k^+ = k^- \neq 0$). Their wavenumbers are pronouncedly different (firstly, in magnitudes and, when $\alpha > 8^0$, in sign) and, therefore, the preferred direction of energy flow (the negative direction of axial coordinate) emerges. Partition of energy flow for $\alpha = 12^0$ is illustrated in Fig. 12(b). The waveguide properties of the shell are transformed again at $\alpha \approx 15^0$. As seen in Fig. 10,

the pair of propagating waves emerges (cuts on) and the lower branch (the 'anomalous' one characterised by the inequality $\frac{\omega}{k}\cdot\frac{d\omega}{dk}<0$) 'collides' with the branch coming from $\alpha=0$ and this pair transforms back (cuts off) to attenuated waves. After this transformation, the preferred direction of the energy flow is reversed, as seen in Fig. 10. The partition of energy flow at $\alpha=18^0$ is shown in Fig. 12(c). As seen in Fig. 10, the structure of dispersion curves remains unchanged up to $\alpha=45^0$. For consistency, the contributions to energy flow at $\alpha=45^0$ are presented in Fig. 12(d). In Fig. 12, each of the four components of the energy flow (10) is presented separately:

$$N^u=\frac{1}{2}\mathrm{Re}\left\{Q_{1\pm}^{F(3)}(x)\cdot\left[i\Omega u_{1\pm}^{F(3)}(x)\right]^*\right\},\ N^v=\frac{1}{2}\mathrm{Re}\left\{Q_{2\pm}^{F(3)}(x)\cdot\left[i\Omega v_{1\pm}^{F(3)}(x)\right]^*\right\},$$

$$N^w=\frac{1}{2}\mathrm{Re}\left\{Q_{3\pm}^{F(3)}(x)\cdot\left[i\Omega w_{1\pm}^{F(3)}(x)\right]^*\right\},\ N^{w'}=\frac{1}{2}\mathrm{Re}\left\{Q_{4\pm}^{F(3)}(x)\cdot\left[i\Omega \gamma_{1\pm}^{F(3)}(x)\right]^*\right\}.$$

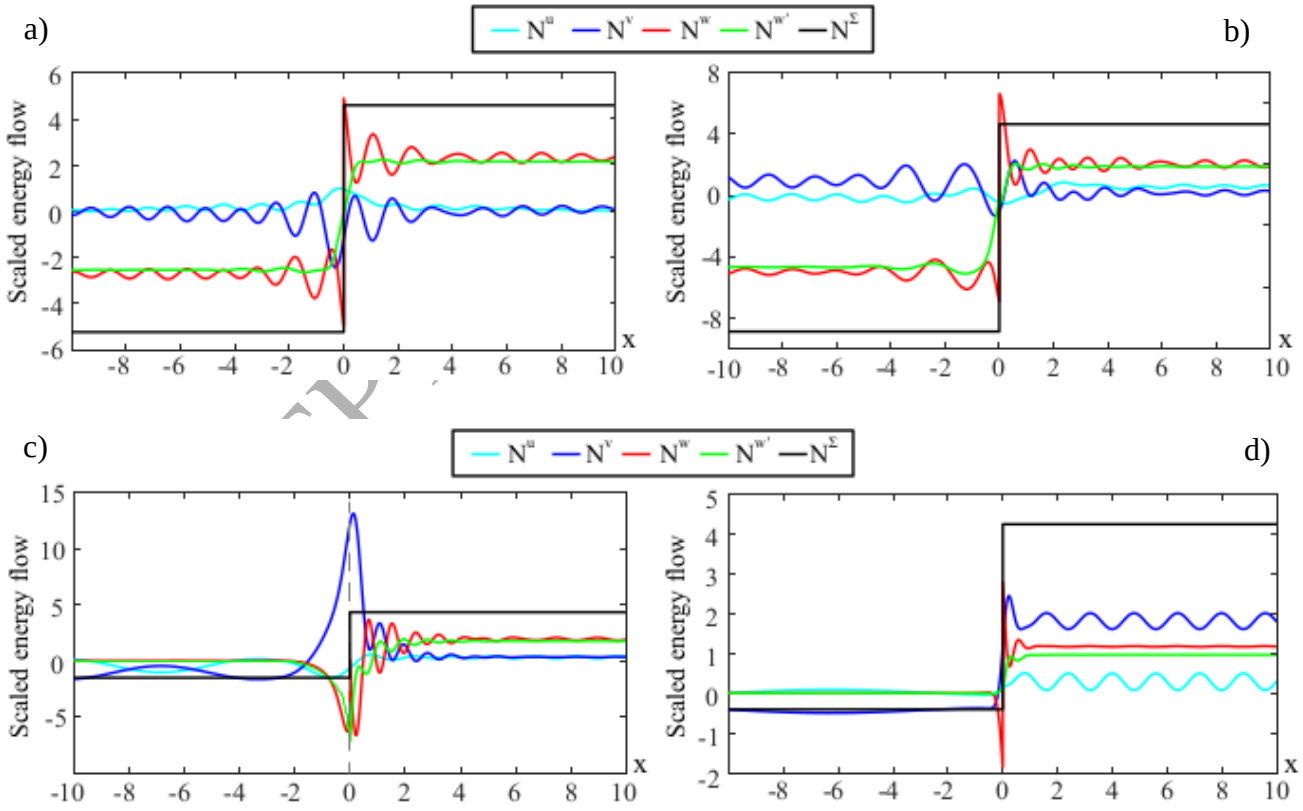

Fig. 12. Partition of the energy flow between alternative paths at $\Omega=0.4$. *(a):* $\alpha=3^0$ *,(b):* $\alpha=12^0$, *(c):* $\alpha=18^0$ *, (d):* $\alpha=45^0$.

Detailed analysis of the energy distribution between alternative transmission paths illustrated in Fig. 12 (a)-(d) lies beyond the scope of this paper, but two remarks should be made. First, the energy input of the radial force is distributed to all transmission paths already at the loaded cross-section, whereas in the isotropic shell and in the cases $\alpha = 0$ or $\alpha = \frac{\pi}{2}$ the energy is pumped only to the directly excited path at $x = x_0$, and it is redistributed in the near field. Second, the energy distribution between alternative transmission paths is not the same in the regions $x < x_0$ and $x > x_0$.

The features of the energy transmission are sensitive to the material parameters of a shell and to the excitation conditions. Therefore, optimization of material layout in order to control energy flow generated by a given rotating force is plausible and may be much beneficial in various applications, for instance, for water-supplying pipes equipped with centrifugal pumps operated at constant speed.

6. CONCLUSIONS

Elastic wave propagation in helically orthotropic cylindrical shells and in helical lattices is studied using an analytical approach and a Wave Finite Element model. Both methods are very efficient in terms of computational cost, theoretical understanding of the wave characteristics and utilisation of the model for parametric studies. Results obtained by these methods are in a good agreement with each other, and contain the aspects of novelty in the following:

1. the analysis of propagation of free waves demonstrates that the symmetry in the location of dispersion curves for an orthotropic cylindrical shell with respect to the $\mathrm{Re}[k] = 0$ plane is broken as soon as the angle α between the principal directions of anisotropy and the cylindrical coordinates depart from its extreme values $\alpha = 0$ and $\alpha = \frac{\pi}{2}$. Mathematically, it is explained by the simple fact that the polynomial dispersion equation contains both the odd and the even powers of the wavenumber. However, the symmetry of dispersion curves for an orthotropic cylindrical shell with respect to the $\mathrm{Im}[k] = 0$ plane is preserved at any α, because the coefficients in the polynomial dispersion equation are purely real so that it may have only complex conjugate roots. As soon as the orthotropy angle acquires the limit values of the pitch angle $\alpha = 0$ or $\alpha = \frac{\pi}{2}$ the odd power vanish, and the symmetry with respect to the $\mathrm{Re}[k] = 0$ plane is recovered. The odd powers also vanish for an arbitrary α if the elastic

parameters describe an isotropic material of the shell. Exactly the same features of the location of dispersion curves are detected for a helical lattice;

2. the non-symmetry of dispersion diagrams with respect to the $\mathrm{Re}[k]=0$ plane is significant for applications, where a cylindrical shell is exposed to the excitation by a rotating force. Solutions of forcing problems in these excitation conditions show that the angle of orientation of principal directions of orthotropy strongly influences partition of the energy flow in the positive and the negative directions of the axial coordinate as well as the energy distribution between alternative transmission paths in each direction. Therefore, the helical orthotropy may be used as a novel efficient tool to tailor the waveguide properties of cylindrical shells in the prescribed direction of wave propagation and, therefore, to control energy flow in piping systems at prescribed excitation frequencies.

REFERENCES

[1] D. Pearson, Dynamic behaviour of helical springs. *The Shock and Vibration Digest*, 20, 3-9, 1988.

[2] S. Sorokin, Linear dynamics of elastic helical springs: Asymptotic analysis of wave propagation. *Proceeding of the Royal Society A: Mathematical, Physical and Engineering Sciences*, 465, 1513–1537, 2009.

[3] J. Lee, D.J. Thompson, Dynamic stiffness formulation, free vibration and wave motion of helical springs. *Journal of Sound and Vibration*, 239, 297-320, 2001.

[4] J. Lee, Free vibration analysis of cylindrical helical springs by the pseudospectral method. *Journal of Sound and Vibration*, 302, 185-196, 2007.

[5] S. Sorokin, The Green's matrix and the boundary integral equations for analysis of time-harmonic dynamics of elastic helical springs. *Journal of the Acoustical Society of America*, 129, 1315-1323, 2011.

[6] J.M. Renno, B.R. Mace, Vibration modelling of helical springs with non-uniform ends. *Journal of Sound and Vibration*, 331, 2809-2823, 2012.

[7] F. Treyssede, Elastic waves in helical waveguides. *Wave Motion*, 45, 457–470, 2008.

[8] Y. Liu, Q. Han, C. Li, H. Huang, Numerical investigation of dispersion relations for helical waveguides using the Scaled Boundary Finite Element method. *Journal of Sound and Vibration*, 333, 1991-2002, 2014.

[9] Yingjing Liang, Yiyi Li, Yijie Liu, Qiang Han, Dianzi Liu, Investigation of wave propagation in piezoelectric helical waveguides with the spectral finite element method. *Composites Part B: Engineering*, 160, 205-216, 2019.

[10] Z. C. Xi, G.R. Liu, K.Y. Lam and H.M. Shang, Dispersion and characteristic surfaces of waves in laminated composite circular cylindrical shells. *Journal of Acoustical Society of America*, 108, 2179-2186, 2000.

[11] J. Kaplunov, A. Nobili, A robust approach for analysing dispersion of elastic waves in an orthotropic cylindrical shell. *Journal of Sound and Vibration*, 401, 23-35, 2017.

[12] V.V. Tyutekin, Helical Waves of an Elastic Cylindrical Shell, *Akusticheskij ZHurnal*, 50, 331-336, 2004 (in Russian).

[13] I.A. Panfilov, Y.A. Ustinov, A study of harmonic fluctuations hollow the cylinder with screw anisotropy on the basis of three dimensional equations of elasticity theory. *Vladikavkazskij matematicheskij Zhurnal*, 13, 35-44, 2011 (in Russian).

[14] I.A. Panfilov, Y.A. Ustinov, Harmonic vibrations and waves in a cylindrical helically anisotropic shell. *Mechanics of Solids*, 47, 195-204, 2012.

[15] E. Manconi, S. Sorokin, R. Garziera, A. Søe-Knudsen, Wave motion and stop-bands in pipes with helical characteristics using Wave Finite Element analysis. *Journal of Applied and Computational Mechanics*, 4, 420-428, 2018.

[16] V.V. Novozhilov, The Theory of Thin Shells, P. Noordhoff Ltd, Groningen, The Netherlands, 1959.

[17] A.L. Gol'denweizer, V.B. Lidskij, P.E. Tovstik, Free Vibration of Thin Elastic Shells, Nauka, Moskva, 1979 (in Russian).

[18] S.A. Ambartsumjan, Theory of Anisotropic Shells, FizMAtGiz, Moscow, p.55, 1961, in Russian

[19] R.M. Jones Mechanics of Composite Materials, Taylor&Francis, Philadelphia, 1999.

[20] B.R. Mace, E. Manconi, Wave motion and dispersion phenomena: veering, locking and strong coupling effects. *Journal of Acoustical Society of America*, 1015-1028, 2012

[21] E. Manconi, B.R. Mace, Veering and Strong Coupling Effects in Structural Dynamics. *Journal of Vibration and Acoustics, Transactions of the ASME*, 139, 021009, 2017

[22] R.D. Mindlin, An Introduction to the Mathematical Theory of Vibrations of Elastic Plates, edited by J. Yang, World Scientific, Singapore (2006).

[23] L.J. Gibson, M.F. Ashby, Cellular Solids: Structure and Properties, 2nd ed, Cambridge: Cambridge University Press, 1997.

[24] S. Gonella, M. Ruzzene, Homogenization and equivalent in-plane properties of two-dimensional periodic lattices. *International Journal of Solids and Structures*, 45, 2897-2915, 2008.

[25] S.M. Jeong, M. Ruzzene, Analysis of vibration and wave propagation in cylindrical grid-like structures. *Shock and Vibration*, 11, 311-331, 2004.

[26] F. Casadei, J.J. Rimoli, Anisotropy-induced broadband stress wave steering in periodic lattices. International. *Journal of Solids and Structures*, 50, 1402-1414, 2013.

[27] P.G. Martinsson, A.B. Movchan; Vibrations of Lattice Structures and Phononic Band Gaps. *The Quarterly Journal of Mechanics and Applied Mathematics*, 56, 45-64, 2003.

[28] S.V. Sorokin, J. Balle Nielsen and N. Olhoff, Green's matrix and the boundary integral equations method for analysis of vibrations and energy flows in cylindrical shells with and without internal fluid loading. *Journal of Sound and Vibration*, 271, 815-847, 2004.

[29] G. Pavic, Vibroacoustical energy flow through straight pipes, *Journal of Sound and Vibration* 154, 411-429, 1992.

[30] M. B. Xu, W.H. Zhang, Vibrational power flow input and transmission in a circular cylindrical shell filled with fluid, *Journal of Sound and Vibration*, 234, 387-403, 2000.

TABLE 1: Wavenumbers in 1/m. Frequency is scaled as $\tilde{\omega} = \frac{\omega}{\Omega_{ring}}$, $\Omega_{ring} = \frac{1}{R}\sqrt{\frac{E_2}{\rho(1-\nu_{12}\nu_{21})}}$

Analytical $m=-1$ $\tilde{\omega}=0.1$	-2.0088	1.5403	24.71 +23.94i	24.71 -23.94i	-24.71 +23.94i	-24.71 -23.94i	0.324 +1.5218i	0.324 -1.5218i
WFEM $m=-1$ $\tilde{\omega}=0.1$	-2.0596	1.6294	25.69 +25.34	25.69 -25.34i	-25.69 +25.34	-25.69 -25.34	0.2129 +1.6209i	0.2129 -1.6209i
Analytical $m=-1$ $\tilde{\omega}=0.6$	-7.6834	5.0445	22.08 +21.58i	22.08 -21.58i	-19.15 +21.61i	-19.15 -21.61i	1.3071 +1.7034i	1.3071 -1.7034i
WFEM $m=-1$ $\tilde{\omega}=0.6$	-7.6445	4.8194	23.35 +22.93i	23.35 -22.93i	-19.47 +23.06i	-19.47 -23.06i	1.2122 +2.2077i	1.2122 2.2077i
Analytical $m=-2$ $\tilde{\omega}=0.1$	-3.1665	2.5961	25.24 +24.83i	25.24 -24.83i	-19.46 +25.18i	-19.46 -25.18i	0.3504 +2.7078i	0.3504 -2.7078i
WFEM $m=-2$ $\tilde{\omega}=0.1$	-3.1300	2.7207	26.53 +26.32i	26.53 -26.32i	-19.26 +26.79i	-19.26 -26.79i	0.3029 +2.8874i	0.3029 -2.8874i
Analytical $m=-2$ $\tilde{\omega}=0.6$	-12.2693	8.3454	22.27 +22.83i	22.27 -22.83i	-16.79 +23.65i	-16.79 -23.65i	2.3289 +5.0535i	2.3289 -5.0535i
WFEM $m=-2$ $\tilde{\omega}=0.6$	-12.1535	8.0039	24.01 +24.16i	24.01 -24.16i	-16.65 +25.13i	-16.65 -25.13i	2.0914 +5.8775i	2.0914 -5.8775i